CHEMISTRY OF MATERIALS

ARTICLE

pubs.acs.org/cm

Neutron and X-ray Diffraction Study of Pyrophosphate-Based $Li_{2-x}MP_2O_7$ (M = Fe, Co) for Lithium Rechargeable Battery Electrodes

Hyungsub Kim,[†,‡] Seongsu Lee,[‡] Young-Uk Park,[§] Haegyeom Kim,[§] Jongsoon Kim,[§] Seokwoo Jeon,[†] and Kisuk Kang*[,§]

[†]Department of Materials Science and Engineering, KAIST, 291 Daehak-ro, Yuseong-gu, Daejeon 305-701, Republic of Korea

[‡]Korea Atomic Energy Research Institute, P.O. Box 105, Yuseong-gu, Daejeon 305-600, Republic of Korea

[§]Department of Materials Science and Engineering, Seoul National University, 599 Gwanak-ro, Gwanak-gu, Seoul 151-742, Republic of Korea

ABSTRACT: Structural characterization of $Li_{2-x}MP_2O_7$ (M = Fe, Co) was carried out using neutron diffraction (ND) and X-ray diffraction (XRD) analyses to elucidate structural information and structural changes during an electrochemical reaction. The crystal system and space group were determined to be monoclinic $P2_1/c$ for both materials with a = 11.0192 (4) Å, b = 9.7488 (3) Å, c = 9.8057 (4) Å, and β = 101.569 (3)° for $Li_{2-x}FeP_2O_7$ and a = 10.9574 (3), b = 9.6921 (3), c = 9.7611 (3), and β = 101.776 (2)° for $Li_{2-x}CoP_2O_7$. XRD analysis revealed partial occupancy of iron and cobalt in the structures of $Li_{2-x}FeP_2O_7$ and $Li_{2-x}CoP_2O_7$, respectively. Also, ND identified lithium positions and partial occupancies in five different Li sites of $Li_{2-x}MP_2O_7$ (M = Fe, Co). Further ex situ XRD showed that the charging/discharging of $Li_{2-x}FeP_2O_7$ occurred primarily via a two-phase reaction with a slight solid solution behavior. We also demonstrated for the first time that $Li_{2-x}CoP_2O_7$ electrodes are electrochemically active, with a redox potential of ~5 V (versus Li).

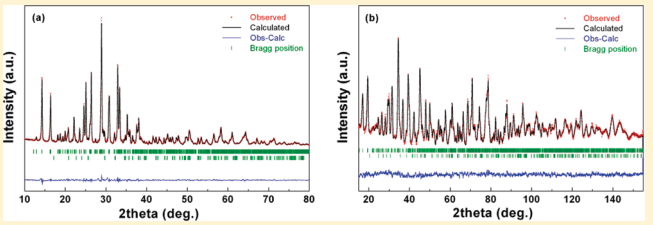

KEYWORDS: structural characterization, neutron diffraction, X-ray diffraction, $Li_{2-x}MP_2O_7$ (M = Fe, Co)

1. INTRODUCTION

Because lithium-ion batteries are being considered as large-scale energy-storage systems (ESSs),[1,2] the search for new electrode materials to replace $LiCoO_2$ is becoming increasingly important. In particular, olivine-structured materials[3−5] such as $LiFePO_4$ are of interest because they are considered safe, which is essential for large-scale battery systems. In addition to olivine materials, other new materials such as fluorinated phosphate,[6] fluorinated sulfate,[7] silicates,[8,9] and NASICON-type electrodes[10−12] have been investigated as alternatives to oxide-based cathode materials, which are costly and subject to safety issues.

Recently, a newly synthesized pyrophosphate-based $Li_2MnP_2O_7$ material was reported.[13] Although the material is electrochemically inactive, Nishimura et al.[14] and Zhou et al.[15] found that the Fe version of pyrophosphate, $Li_2FeP_2O_7$, is a promising 3.5 V class cathode material for lithium-ion batteries and can safely deliver high-energy density. Nishimura et al. also determined the structure of lithium iron pyrophosphate using synchrotron X-ray diffraction (XRD), which suggested a quasi two-dimensional network of lithium paths. However, lithium sites and occupancy were not sufficiently characterized. Due to the low scattering of lithium in XRD, the decisive lithium environments in the structure could not be assured especially when various Li sites are present in $Li_{2-x}MP_2O_7$ (M = Fe, Co). Precise determination of the electrode material structure is important for understanding and exploiting electrochemical behavior in battery systems.[16,17]

Here, we report the detailed structural characterization of $Li_{2-x}MP_2O_7$ (M = Fe, Co). Atomic sites and occupancies were determined by Rietveld refinements of neutron diffraction (ND) and XRD. Whereas XRD analysis is sensitive to transition metals (TMs) and atoms with high atomic numbers, the sensitivity of ND to lithium enabled us to determine the exact lithium positions and occupancies. Combined XRD and ND studies are advantageous for characterizing Li-ion battery electrode materials.[18−20] Furthermore, we propose $Li_{2-x}CoP_2O_7$, which is isostructural to $Li_{2-x}MP_2O_7$ (M = Mn, Fe), as a new cathode for lithium rechargeable batteries.

2. EXPERIMENTAL SECTION

2.1. Synthesis. Lithium TM pyrophosphate $Li_{2-x}MP_2O_7$ (M = Fe, Co) samples were synthesized using a two-step solid-state method. The starting materials were Li_2CO_3 (ACS reagent, ≥99%, Aldrich), $FeC_2O_4 \cdot 2H_2O$ (99%, Aldrich), $CoC_2O_4 \cdot 2H_2O$ (Reagent grade, Alfa Aesar), and $(NH_4)_2HPO_4$ (ACS reagent 98%, Aldrich). We did not use enriched ^7Li or ^6Li samples. These precursors were mixed by ball milling with acetone for 24 h. After the acetone was allowed to evaporate at 70 °C for 12 h, the mixture was ground. The ground powder was initially heated at 300 °C for 6 h under Ar flow. The calcined sample was reground and pelletized manually under 200 kg·cm^{-2} pressure using a disk-shaped mold. The pelletized sample was calcined again at 550−600 °C for 10 h under Ar flow.

Received: May 8, 2011
Revised: July 26, 2011
Published: August 18, 2011

To prepare $LiFeP_2O_7$, $Li_{2-x}FeP_2O_7$ was chemically delithiated using NO_2BF_4 (Aldrich, 95%) in acetonitrile solvents (99%, Aldrich) according to the following reaction

$$Li_{2-x}FeP_2O_7 + NO_2BF_4 \rightarrow LiFeP_2O_7 + LiBF_4 + NO_2$$

NO_2BF_4 was used as a strong oxidizing agent with a redox potential for NO_2^+/NO_2 of 5.1 V versus Li^+/Li.[21,22] The solution was stirred for 12 h at 60 °C. The final product, $LiFeP_2O_7$, was obtained by washing reactants several times with acetonitrile using a centrifuge.

2.2. Characterization. Positions and partial occupancies of TMs (Co or Fe) in the synthesized $Li_{2-x}MP_2O_7$ (M = Fe, Co) were determined using an X-ray diffractometer (Rigaku, D/MAX 2500) equipped with Cu Kα radiation (λ = 1.5406 Å). Data were recorded over a 2θ range of 10 to 80°, with a step size of 0.02°. Each step was exposed for 4 s. ND analysis of $Li_{2-x}MP_2O_7$ (M = Fe, Co) was carried out to determine lithium positions and occupancies. ND data were collected over a 2θ range of 0−180° with a step size of 0.05°, and λ = 1.8348 Å was supplied by a Ge (331) single-crystal monochromator on a high-resolution powder diffractometer (HRPD) at the HANARO facility at the Korea Atomic Energy Research Institute. Further XRD analysis was performed to investigate structural evolution during charging and discharging. The data were collected over a 2θ range of 10−60° with a step size of 0.02° using the same X-ray diffractometer (Rigaku, D/MAX 2500). ND and XRD data were refined by the Rietveld method using Fullprof software.[23] Samples were further characterized using a Fourier transform infrared (FT-IR) microscope (Hyper ion 3000) by KBr pellet analysis. Atomic ratios of elements such as Li, Fe, and Co in $Li_{2-x}FeP_2O_7$, $LiFeP_2O_7$, and $Li_{2-x}CoP_2O_7$ were determined by inductively coupled plasma−atomic-emission spectroscopy (ICP−AES, Thermo Jarrel Ash, Polyscan 60E, USA). Thermal gravimetric analysis (TGA) and differential scanning calorimetry (DSC) were used to investigate the structural stability of the delithiated sample at various temperatures using a Setsys16/18 thermogravimetry analyzer (SETARAM, France) under an Ar atmosphere at a heating rate of 10 °C·min^{-1} from room temperature to 600 °C.

2.3. Electrochemical Tests. Electrochemical tests were performed in a CR2016-type coin cell assembled in an Ar-filled glovebox. The electrode was prepared as follows. First, the powder was mixed with super P by dry ball milling at a ratio of 85:15 wt %. Then, the total composition of the electrode was adjusted to 70 wt % of the active material, 20 wt % super P, and 10 wt % polyvinylidene fluoride (PVDF). The electrode was fabricated by pasting a slurry of the powder mixture in *N*-methyl-2-pyrrolidone (99.5%, Aldrich) (NMP) onto Al foil using a doctor blade. NMP was evaporated for 2 h in an oven at 110 °C. The loading amount of the electrode was 1.95 × 10^{-3} g cm^{-2}. The cell was assembled using a Li counter electrode (Hohsen Corp, Japan), a separator (Celgard 2400), and 1 M solution of $LiPF_6$ in ethyl carbonate/dimethylcarbonate (EC/DMC, 1:1 v/v, Techno Semichem) in an Ar-filled glovebox. Cyclic voltammetry (CV) was performed over the voltage range of 2.0−5.5 V for $Li_{2-x}CoP_2O_7$ at room temperature using Solartron. The CV measurement was performed at a scan rate of 0.02 mV s^{-1}. Galvanostatic charge/discharge tests were performed at various C rates (2C, 1C, C/2, C/5, C/10, C/20, i.e., 5 ∼ 250 mA g^{-1}) for $Li_{2-x}FeP_2O_7$. Quasi-open-circuit potential (QOCP) tests on the $Li_{2-x}FeP_2O_7$ sample were performed at a C/50 rate with 2 h relaxation time using an intermittent charge/discharge mode.[24] After the relaxation, dV/dt was below 10^{-6} V s^{-1}.

3. RESULTS AND DISCUSSION

3.1. Structural Characterization. We investigated the structures of $Li_{2-x}FeP_2O_7$ and $Li_{2-x}CoP_2O_7$ using XRD and ND analyses. Figure 1(a−d) shows the XRD and ND patterns of $Li_{2-x}FeP_2O_7$ (Figure 1(a), (b)) and $Li_{2-x}CoP_2O_7$ (Figure 1(c),

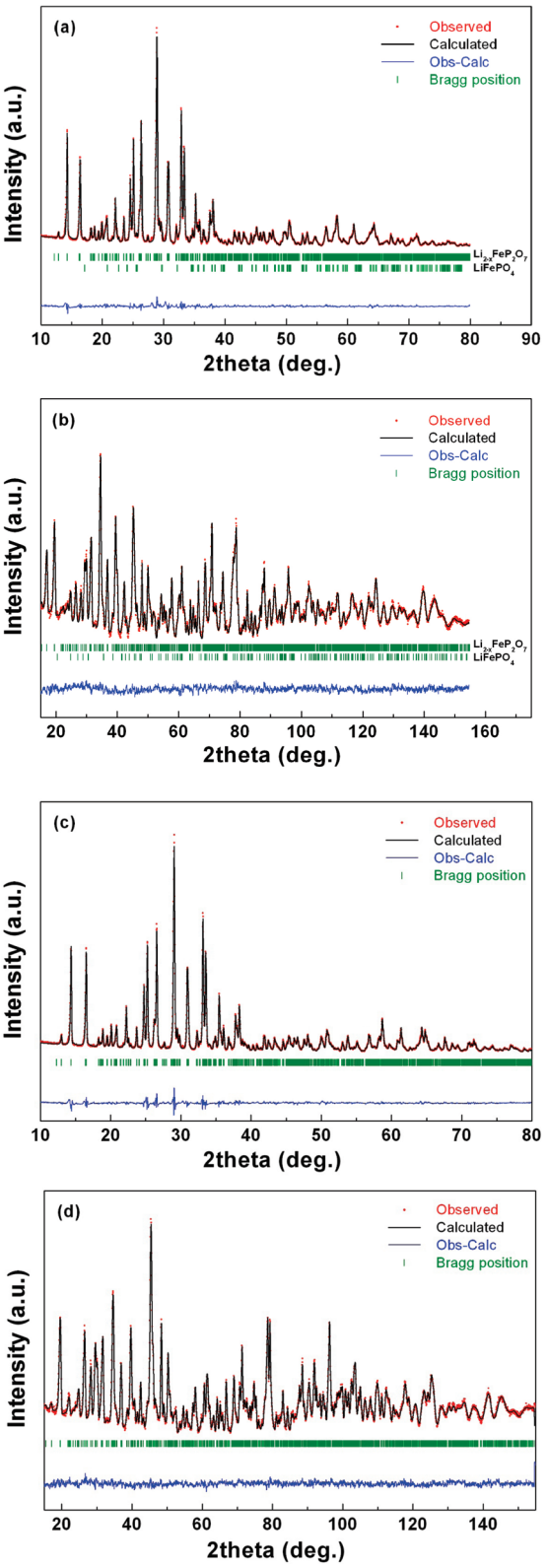

Figure 1. Rietveld refinements of the (a) XRD and (b) ND patterns of $Li_{2-x}FeP_2O_7$ with $Li_{2-x}CoP_2O_7$ (c) XRD and (d) ND patterns. *R*-factors for (a) XRD pattern are R_p = 3.28%, R_I = 1.97%, R_F = 1.15%, S = 2.14. and those for (b) ND pattern are R_p = 2.10%, R_I = 3.30%, R_F = 1.61%, S = 1.75. *R*-factors for (c) XRD and ND patterns of $Li_{2-x}CoP_2O_7$ are R_p = 4.29%, R_I = 2.77%, R_F = 2.07, S = 2.43 and R_p = 2.16%, R_I = 2.75%, R_F = 1.48%, S = 1.48, respectively.

dx.doi.org/10.1021/cm201305z |*Chem. Mater.* 2011, 23, 3930–3937

Table 1. Refined Lattice Parameters from XRD and ND Patterns

designation	description	a (Å)	b (Å)	c (Å)	β (deg)	vol
$Li_{2-x}FeP_2O_7$	X-ray	11.0224 (4)	9.7541 (3)	9.8080 (3)	101.564 (2)	1033.083
	neutron	11.0192 (4)	9.7488 (3)	9.8057 (4)	101.569 (3)	1032.097
	ref 14	11.0185	9.7553	9.8052	101.542	1033.01
$Li_{2-x}CoP_2O_7$	X-ray	10.9603 (3)	9.6957 (2)	9.7641 (2)	101.784 (1)	1015.740
	neutron	10.9574 (3)	9.6921 (3)	9.7611 (3)	101.776 (2)	1014.810

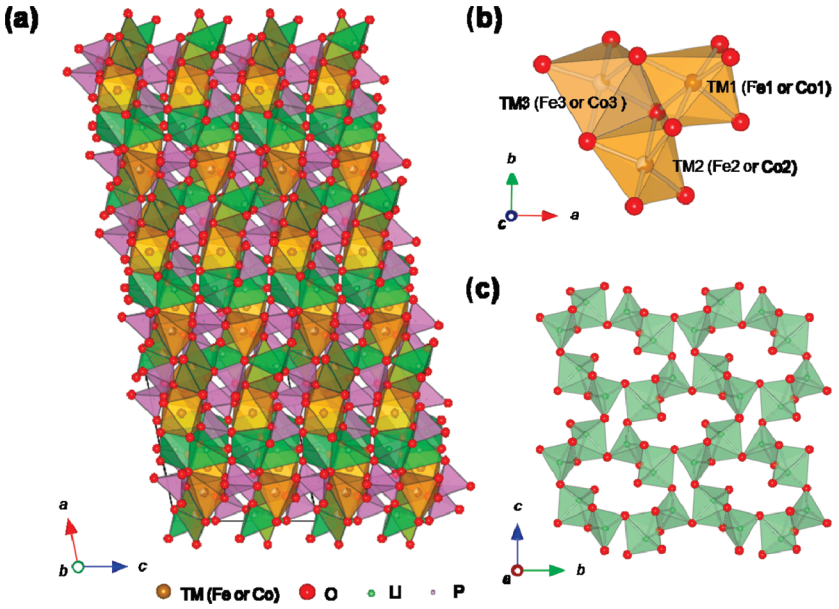

Figure 2. Schematic representation of the structure of $Li_{2-x}MP_2O_7$ (M = Fe, Co).

(d)). Below the measured diffraction patterns are the calculated patterns for each phase and the difference between the calculated and observed patterns. The crystal system and space group were determined to be monoclinic $P2_1/c$ for both materials, consistent with previous reports on lithium iron and manganese pyrophosphate-based materials.[13−15]

Table 1 shows the refined lattice parameters of $Li_{2-x}FeP_2O_7$ and $Li_{2-x}CoP_2O_7$ from XRD and ND along with previously reported values for $Li_{2-x}FeP_2O_7$. $Li_{2-x}FeP_2O_7$ XRD values were close to the ND values and were consistent with previous XRD results.[14] Refinement of $Li_{2-x}CoP_2O_7$ resulted in lattice parameters of a = 10.9603 (3) Å, b = 9.6957 (2) Å, c = 9.7641 (2) Å, and β = 101.784 (1)° from XRD. This result is comparable to previous structure reports on $Li_{4+x}Co_{2-x}(P_2O_7)_2$.[25] The lattice parameters of $Li_{2-x}CoP_2O_7$ are smaller than those of $Li_{2-x}FeP_2O_7$ due to the smaller ionic size of Co^{2+} (0.745 Å, high spin) compared with Fe^{2+} (0.78 Å, high spin).[26] $LiFePO_4$ impurity was detected in the $Li_{2-x}FeP_2O_7$ phase, and the quantitative analysis revealed that ∼3 wt % $LiFePO_4$ was present in the sample. A schematic illustration of the refined structures is shown in Figure 2. In $Li_{2-x}MP_2O_7$ (M = Fe, Co), the TM polyhedra are edge shared, and the three polyhedra are interconnected with P_2O_7 via corner sharing. Iron and cobalt-based pyrophosphate materials are isostructural to $Li_2MnP_2O_7$, except for TM partial occupancy in Li sites and Li partial occupancy in TM sites.[13] Three different TM sites and five different Li sites are present in the crystal structure. TM1 sites are in TMO_6 distorted octahedra, and TM2 and TM3 sites are in TMO_5 bipyramids with partial occupancies (Figure 2(b)). TM atoms were refined to be intermixed with Li atoms in TM2 and TM3 sites for both $Li_{2-x}FeP_2O_7$ and $Li_{2-x}CoP_2O_7$. Quantitative analysis on partial occupancy is discussed later. Among five Li sites, Li1 and Li2 are tetrahedrally coordinated; Li3 forms bipyramidal sites; Li4 shares its occupancy with TM3 bipyramids; and Li5 shares its occupancy with TM2 bipyramids. Li sites (Li1, Li2, Li3, Li4) in both $Li_{2-x}FeP_2O_7$ and $Li_{2-x}CoP_2O_7$ are two-dimensionally linked toward the b- and c-axes. These quasi two-dimensional lithium links are expected to provide lithium-ion diffusion paths (Figure 2(c)).

Prior to quantitative analysis of partial occupancies in the crystal, the effect of partial occupancies of TMs and Li on the relative intensities of diffraction peaks was examined by simulating XRD patterns and ND patterns, respectively. The evolution of simulated peaks according to Fe partial occupancy is presented in Figure 3(a) for XRD, and that of Li partial occupancy is shown in Figure 3(b) for ND. Fe partial occupancy simulations were carried out by changing the relative ratio of Fe2 and Fe3 (Fe2 + Fe3 = 1) in the crystal. As shown in Figure 3(a), (110), (011), (−111), and (200) peaks strongly depended on the relative occupancies of Fe2 and Fe3 sites. In particular, the (−111) peak intensity decreased significantly with increasing Fe2 partial occupancy. The relative intensity ratio (I (−111)/I (200)) decreased from 1.922 to 0.498 as Fe2 occupancy increased from 0.5 to 1.0. The lowest R-factors with respect to Fe2/Fe3 partial occupancy were obtained for the model with Fe2 = 0.67 (Fe3 = 0.33). Partially occupied lithium models were also analyzed by simulating the effect of Li4 partial occupancy in the ND pattern.

dx.doi.org/10.1021/cm201305z |*Chem. Mater.* 2011, 23, 3930–3937

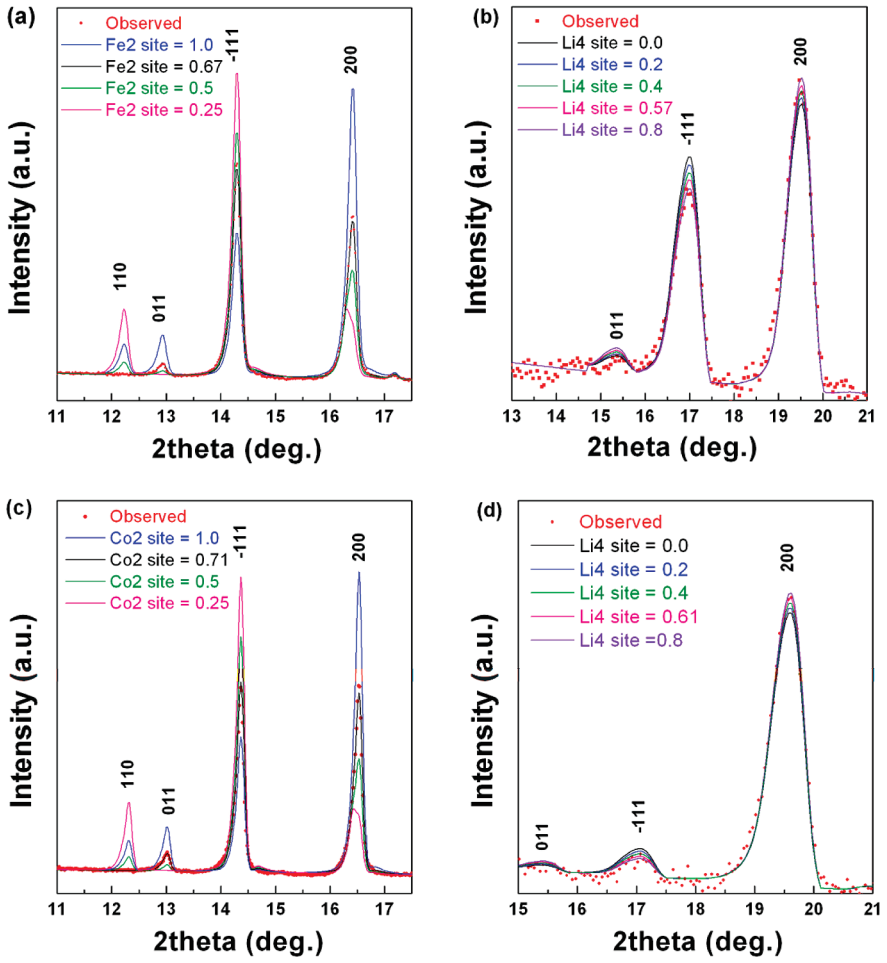

Figure 3. Simulated (a) XRD and (b) ND patterns of $Li_{2-x}FeP_2O_7$ as a function of partial occupancy of Fe and Li. Simulated (c) XRD and (d) ND patterns of the $Li_{2-x}CoP_2O_7$ according to the partial occupancy of Co and Li.

Variation in the (011), (−111), and (200) peak intensities was observed with varying Li4 occupancy in Figure 3(b). The relative intensity ratio between the (−111) and (200) peaks decreased from 0.692 to 0.616 as Li4 occupancy increased from 0.4 to 0.8. The refined patterns showed the lowest *R*-factors when Li partial occupancies were 0.63 for the Li4 site and 0.94 for the Li3 site, indicating a slight lithium deficiency in the structure.

Similar simulations were also performed for the newly synthesized $Li_{2-x}CoP_2O_7$ phase, as shown in Figure 3(c) and 3(d). The trend of (110), (011), (−111), and (200) peak intensity variation was similar to that of $Li_{2-x}FeP_2O_7$ for various partial occupancies of Co2 and Co3 (Figure 3(c)). The lowest *R*-factors were obtained when Co2 occupancy was 0.71 from the refined XRD pattern. ND pattern simulations verified the partial occupancy of Li4. The variation in Li4 occupancy changed the relative intensity ratio of (011), (−111), and (200) (Figure 3(d)). The lowest *R*-factors were obtained for the partial occupancy of Li4 = 0.65.

Final refined atomic positions and occupancy with thermal factors from combined XRD and ND analyses are listed in Tables 2 and 3 for $Li_{2-x}FeP_2O_7$ and $Li_{2-x}CoP_2O_7$, respectively. The partial occupancy of Fe was 0.67 in Fe2 sites and 0.33 in Fe3 sites, and Fe3 sites were intermixed with 0.63 Li (Li4 sites) in $Li_{2-x}FeP_2O_7$. The Co2:Co3 partial occupancy ratio was 0.71:0.29, and Li occupancy in Co3 sites (Li4 sites) was refined to be 0.65 in $Li_{2-x}CoP_2O_7$. Also, slight Li deficiency in the Li3 site was detected as 0.94 for $Li_{2-x}FeP_2O_7$ and 0.91 for $Li_{2-x}CoP_2O_7$. As shown in Tables 2 and 3, both $Li_{2-x}FeP_2O_7$ and $Li_{2-x}CoP_2O_7$ phases exhibited some degree of Li deficiency. Moreover, ICP−AES analysis revealed that the atomic ratios of Fe/Li and Co/Li were 1.89 and 1.81 in $Li_{2-x}FeP_2O_7$ and $Li_{2-x}CoP_2O_7$, respectively, consistent with XRD and ND results.

For further examination of $Li_{2-x}MP_2O_7$ (M = Fe, Co), FT-IR analysis was performed (Figure 4). P−O−P and O−P−O bonds and PO_3 bonds in $(P_2O_7)^{4-}$ are clearly observed in the FT-IR spectra for both $Li_{2-x}MP_2O_7$ (Fe or Co). A symmetric vibration (ν_s) of P−O−P bonds in $Li_{2-x}FeP_2O_7$ was measured at 746.23 cm^{-1}, and an asymmetric vibration (ν_{as}) was measured at 944.85 cm^{-1}. ν_s and ν_{as} of P−O−P bonds in $Li_{2-x}CoP_2O_7$ were shifted to 750.61 and 942.61 cm^{-1}, respectively. The vibrations of P−O bonds in PO_3 were observed in the range of 850−990 cm^{-1} for ν_s and 990−1400 cm^{-1} for ν_{as}. Those of O−P−O bonds were observed in the range of 400−645 cm^{-1}. These results are consistent with previous reports on other alkali pyrophosphate-based materials.[27,28]

3.2. Structural Evolution during Charging/Discharging and Stability of the Charged Sample. We investigated the structural evolution of $Li_{2-x}FeP_2O_7$ electrodes in a Li cell using ex situ XRD analysis. At a low current rate, the $Li_{2-x}FeP_2O_7$ electrode delivered ~110 mAh g^{-1}, which is close to its theoretical capacity (Figure 5(a)).[14] XRD measurements were carried out in

dx.doi.org/10.1021/cm201305z |*Chem. Mater.* 2011, 23, 3930–3937

Table 2. Atomic Position and Occupancy of Refined $Li_{2-x}FeP_2O_7$ Using ND Patterns

atom	multiplicity	x	y	z	B_{iso}	occupancy
Fe1	4	0.6723(4)	0.5715(5)	0.6947(4)	1.19(7)	1.00
Fe2	4	0.8233(6)	0.2872(6)	0.7557(7)	1.19(7)	0.67(2)
Li5	4	0.8233(6)	0.2872(6)	0.7557(7)	1.19(7)	0.18(3)
Fe3	4	0.0369(17)	0.069(2)	0.655(2)	1.19(7)	0.33(1)
P1	4	0.5737(8)	0.6480(7)	0.3764(7)	0.54(8)	1.00
P2	4	0.2456(6)	0.5689(7)	0.5650(7)	0.54(8)	1.00
P3	4	0.8894(7)	0.7976(7)	0.6159(8)	0.54(8)	1.00
P4	4	0.7577(7)	0.0434(7)	0.5258(8)	0.54(8)	1.00
O1	4	0.8548(7)	0.1370(6)	0.6183(8)	1.05(4)	1.00
O2	4	0.7863(7)	0.0319(7)	0.3739(8)	1.05(4)	1.00
O3	4	0.3750(7)	0.5841(8)	0.9843(7)	1.05(4)	1.00
O4	4	0.1091(6)	0.5658(8)	0.5693(8)	1.05(4)	1.00
O5	4	0.6909(6)	0.3244(7)	0.3385(7)	1.05(4)	1.00
O6	4	0.7335(6)	0.4132(7)	0.5859(7)	1.05(4)	1.00
O7	4	0.0727(7)	0.2754(6)	0.0159(7)	1.05(4)	1.00
O8	4	0.4156(7)	0.2902(7)	0.1869(7)	1.05(4)	1.00
O9	4	0.8459(7)	0.6667(7)	0.6833(7)	1.05(4)	1.00
O10	4	−0.0058(6)	0.8669(6)	0.7157(8)	1.05(4)	1.00
O11	4	0.4817(7)	0.9339(7)	0.7775(7)	1.05(4)	1.00
O12	4	0.5528(7)	0.6609(7)	0.5243(8)	1.05(4)	1.00
O13	4	0.2922(6)	0.0744(7)	0.1168(6)	1.05(4)	1.00
O14	4	0.2258(6)	0.1038(7)	0.4004(7)	1.05(4)	1.00
Li1	4	0.445(2)	0.727(3)	0.106(2)	2.3(3)	1.00
Li2	4	0.972(2)	0.625(2)	0.429(3)	2.3(3)	1.00
Li3	4	0.436(2)	0.584(3)	0.813(3)	2.3(3)	0.94(3)
Li4	4	0.0369(17)	0.069(2)	0.655(2)	1.19(7)	0.63(2)

Table 3. Atomic Position and Occupancy of Refined $Li_{2-x}CoP_2O_7$ Using ND Patterns

atom	multiplicity	x	y	z	B_{iso}	occupancy
Co1	4	0.6737(11)	0.5704(14)	0.6977(12)	1.3(2)	1
Co2	4	0.823(2)	0.285(2)	0.756(3)	1.3(2)	0.71(1)
Li5	4	0.823(2)	0.285(2)	0.756(3)	1.3(2)	0.15(2)
Co3	4	0.051(6)	0.096(8)	0.665(8)	1.3(2)	0.29(3)
P1	4	0.5776(6)	0.6504(6)	0.3761(6)	0.55(5)	1.00
P2	4	0.2433(5)	0.5702(6)	0.5636(6)	0.55(5)	1.00
P3	4	0.8877(5)	0.7945(6)	0.6176(6)	0.55(5)	1.00
P4	4	0.7582(5)	0.0466(6)	0.5200(6)	0.55(5)	1.00
O1	4	0.8552(5)	0.1373(5)	0.6132(6)	0.97(3)	1.00
O2	4	0.7857(5)	0.0327(5)	0.3750(6)	0.97(3)	1.00
O3	4	0.3754(5)	0.5841(6)	0.9808(6)	0.97(3)	1.00
O4	4	0.1056(4)	0.5685(6)	0.5706(6)	0.97(3)	1.00
O5	4	0.6900(5)	0.3210(5)	0.3368(5)	0.97(3)	1.00
O6	4	0.7353(5)	0.4126(5)	0.5856(5)	0.97(3)	1.00
O7	4	0.0777(5)	0.2771(5)	0.0238(6)	0.97(3)	1.00
O8	4	0.4148(5)	0.2907(5)	0.1859(6)	0.97(3)	1.00
O9	4	0.8451(5)	0.6656(5)	0.6786(5)	0.97(3)	1.00
O10	4	−0.0032(5)	0.8641(5)	0.7165(6)	0.97(3)	1.00
O11	4	0.4811(5)	0.9349(6)	0.7757(5)	0.97(3)	1.00
O12	4	0.5569(5)	0.6573(5)	0.5271(6)	0.97(3)	1.00
O13	4	0.2916(5)	0.0768(5)	0.1169(5)	0.97(3)	1.00
O14	4	0.2289(4)	0.1046(5)	0.4046(5)	0.97(3)	1.00
Li1	4	0.444(2)	0.7336(19)	0.1144(19)	2.6(2)	1.00
Li2	4	0.9728(17)	0.6167(18)	0.416(2)	2.6(2)	1.00
Li3	4	0.4544(18)	0.568(2)	0.820(2)	2.6(2)	0.91(3)
Li4	4	0.051(6)	0.096(8)	0.665(8)	1.3(2)	0.65(2)

dx.doi.org/10.1021/cm201305z |*Chem. Mater.* 2011, 23, 3930–3937

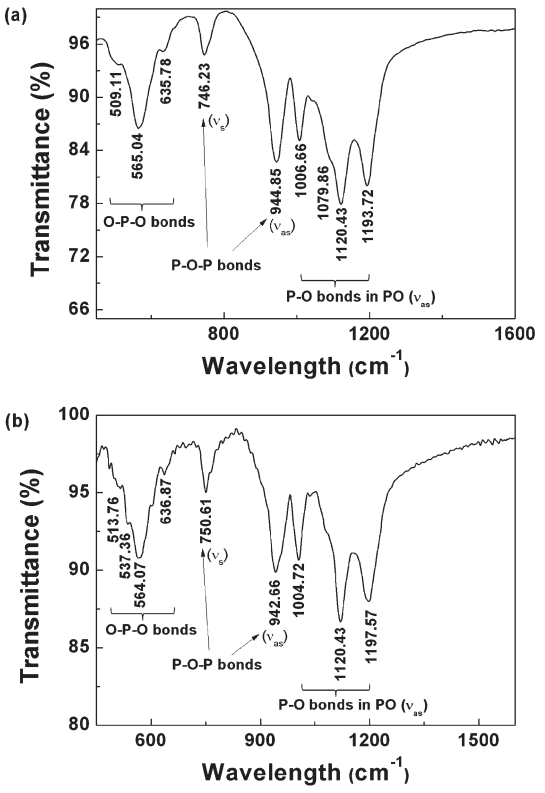

Figure 4. FT-IR spectra of (a) $Li_{2-x}FeP_2O_7$ and (b) $Li_{2-x}CoP_2O_7$.

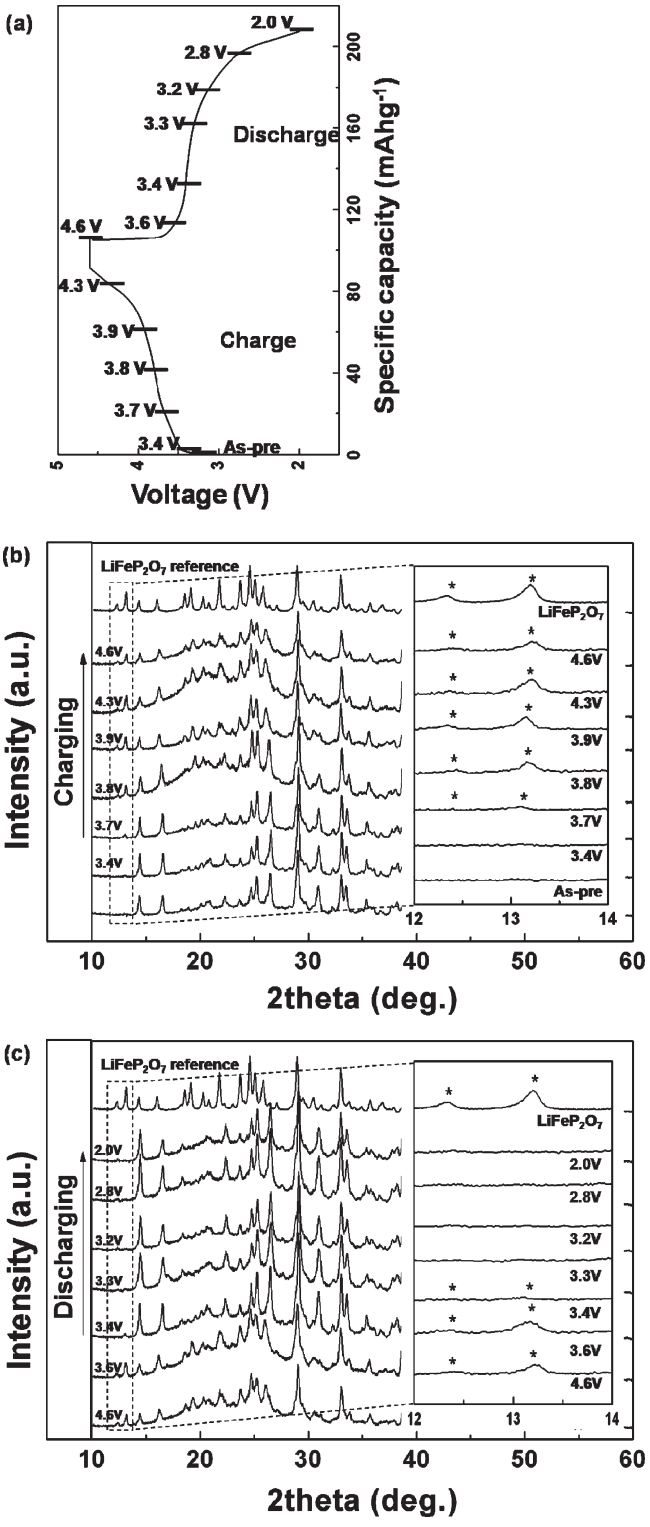

Figure 5. (a) Charge and discharge profiles based on ex situ XRD patterns of $Li_{2-x}FeP_2O_7$ during (b) charging and (c) discharging.

different charge or discharge states, as shown in Figure 5(a). Corresponding XRD patterns are shown in Figure 5(b) and 5(c) for charging and discharging, respectively. During charging, a new set of peaks appeared and grew. In particular, the amplified figure in the inset of Figure 5(b) clearly shows that new peaks at 12 and 13° emerged during charging. To identify these new peaks, we independently synthesized $LiFeP_2O_7$ as a reference by chemical delithiation of $Li_{2-x}FeP_2O_7$ and plotted both XRD patterns in Figure 5(b) and 5(c). The new peaks denoted as (*) correspond to the (110) and (011) peaks of $LiFeP_2O_7$. This observation indicates that the delithiation of $Li_{2-x}FeP_2O_7$ occurred via a two-phase reaction between $Li_{2-x}FeP_2O_7$ and $LiFeP_2O_7$. It should be noted that at the initial stages of charge slight peak shifts occur, implying some degree of solid solution behavior. In the discharge profile, the opposite phenomenon was observed. The (110) and (011) peak intensities decreased reversibly with lithiation. This two-phase reaction of de/lithiation is similar to the behavior of other polyanion electrodes such as $LiFePO_4$ and $LiFeSO_4F$.[3,7]

The fully charged sample, $LiFeP_2O_7$, was further analyzed. Using TGA/DSC measurements, thermal-phase stability of $LiFeP_2O_7$ was examined. Figure 6 shows the thermal behavior when the sample was heated to 600 °C. The delithiated phase, $LiFeP_2O_7$, was stable until 500 °C, with only a slight weight loss of ~5%. A highly exothermal reaction was observed above 510 °C. The stability of the $LiFeP_2O_7$ electrode was comparable to that of charged olivine $LiFePO_4$.[29] However, a detailed phase transformation mechanism should be elucidated.

3.3. Electrochemical Characterization. Figure 7 shows the QOCP measurement at a C/50 rate in intermittent charge/discharge mode. Two hours of relaxation time is applied during each charging and discharging step. After a 2 h rest period, the dV/dt was below 10^{-6} V s^{-1}, indicating that further relaxation would not change the potential significantly. The small polarization at each step indicates that a relatively fast charge/discharge reaction is possible for $Li_{2-x}FeP_2O_7$. In addition to a clear two-phase region in the profile, there is a long, sloping region at the initial delithiation stage. This implies that some degree of solid solution was present in $Li_{2-x}FeP_2O_7$ before the two-phase reaction occurred.[30,31]

dx.doi.org/10.1021/cm201305z |*Chem. Mater.* 2011, 23, 3930–3937

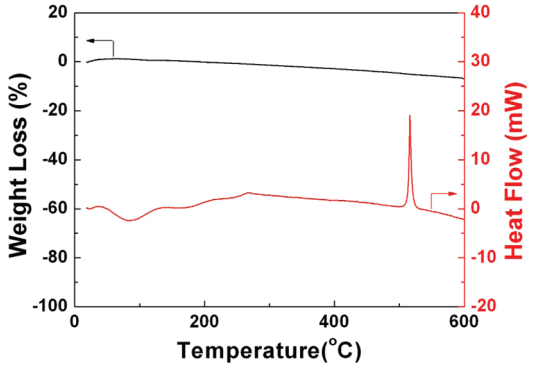

Figure 6. TGA/DSC analysis of delithiated $LiFeP_2O_7$.

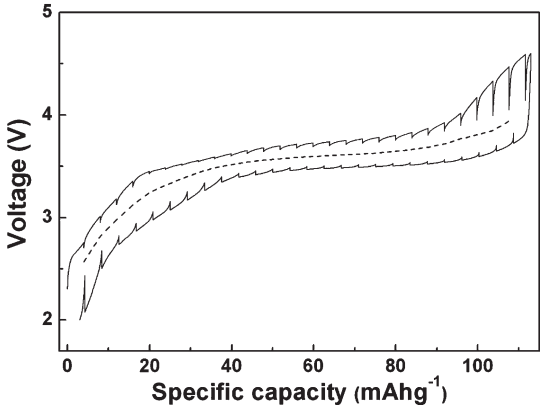

Figure 7. Quasi-open-circuit potential measurement of $Li_{2-x}FeP_2O_7$ during charging/discharging.

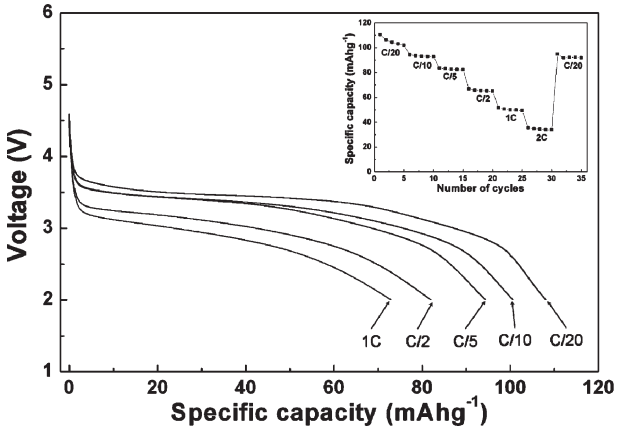

Figure 8. Discharge curves of $Li_{2-x}FeP_2O_7$ as a function of C rate. The inset shows a cyclability graph at various rates.

Further galvanostatic charge/discharge measurements were conducted for the $Li_{2-x}FeP_2O_7$ electrode. Figure 8 shows the initial discharge profiles of the $Li_{2-x}FeP_2O_7$ electrode measured at various current rates (C/20, C/10, C/5, C/2, 1C). At C/20, a capacity close to its theoretical capacity (110 mAh g^{-1}) was achieved. About 65% of the theoretical capacity was retained at a rate of 1C. The cycle performances of $Li_{2-x}FeP_2O_7$ measured at various C rates are shown in the inset of Figure 8. Relatively good cycle performance was observed for each rate. About 100 mAh g^{-1} was retained after 30 cycles of the rate test. The good cycle life was attributed to the stable polyanion framework of $Li_{2-x}FeP_2O_7$ even in the delithiated phase, as previously demonstrated.

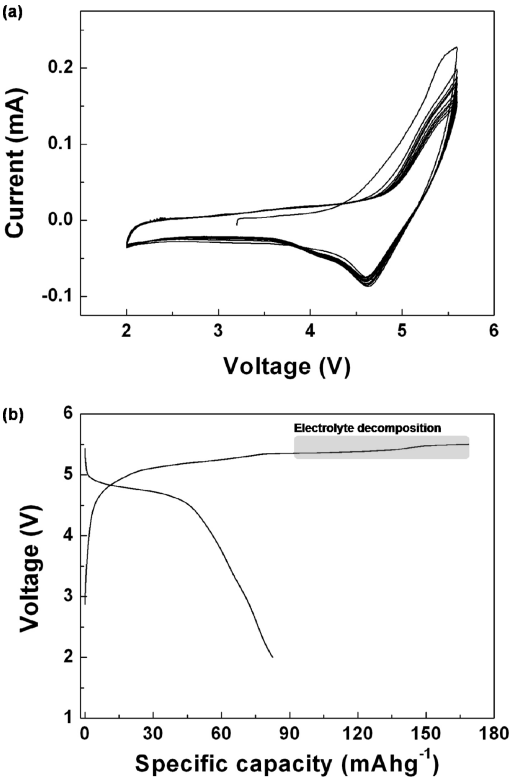

Figure 9. (a) Cyclic voltammogram and (b) charge/discharge curves of $Li_{2-x}CoP_2O_7$.

The electrochemical properties of the newly synthesized $Li_{2-x}CoP_2O_7$ phase were investigated by CV and galvanostatic charge/discharge measurements. The electrochemical properties of $Li_{2-x}CoP_2O_7$ have not been reported previously. Figure 9(a) clearly demonstrates that the $Li_{2-x}CoP_2O_7$ electrode is electrochemically active in a Li cell. Reversible cathodic and anodic peaks were observed between 4.5 and 5.5 V for multiple cycles. Average voltage was estimated to be ~4.9 V. From the galvanostatic measurement in Figure 9(b), the charge/discharge behavior of $Li_{2-x}CoP_2O_7$ was more evidently demonstrated. Charge was extracted from the $Li_{2-x}CoP_2O_7$ electrode at ~5.2 V, along with partial electrolyte decomposition. Upon discharge, about 85 mAh g^{-1} of capacity was reversibly delivered at ~4.8 V, indicating that the charge capacity was not simply due to electrolyte oxidation but also involved a reversible reaction such as lithium extraction and insertion. It should be noted that the redox potential of $Li_{2-x}CoP_2O_7$ is higher than that of $LiCoPO_4$ by ~0.1−0.2 V. This difference is similar to the voltage gap between $Li_{2-x}FeP_2O_7$ (3.5 V) and $LiFePO_4$ (3.4 V).[14] It confirms that the redox potential of the electrode material is sensitive to the crystal structure and the local atomic environment. Although a 4.9 V cathode may not be practical due to the instability of conventional electrolytes at such a high voltage, we believe this material can be used as a cathode when high-voltage electrolytes are developed in the future.

4. CONCLUSIONS

Detailed structural characterization of $Li_{2-x}MP_2O_7$ (M = Fe, Co) was performed by combined ND and XRD analyses. Structural

dx.doi.org/10.1021/cm201305z |Chem. Mater. 2011, 23, 3930–3937

simulations revealed TM and Li partial occupancies. Intermixed TM3 and Li4 sites were carefully analyzed using ND and XRD patterns. Structural evolution of a $Li_{2-x}FeP_2O_7$ electrode in a Li cell occurred via a two-phase reaction, as confirmed by ex situ XRD. The delithiated phase was thermally stable up to 500 °C. We also reported the structure of a newly synthesized phase, $Li_{2-x}CoP_2O_7$, based on ND and XRD analyses. We showed that the $Li_{2-x}CoP_2O_7$ electrode is electrochemically active with a redox potential of ~4.9 V. The $Li_{2-x}CoP_2O_7$ electrode delivered ~85 mAh g^{-1} on discharge at C/20.

AUTHOR INFORMATION

Corresponding Author

*E-mail: matlgen1@snu.ac.kr. Tel.: +82-2-880-7165. Fax: +82-2-880-9617.

ACKNOWLEDGMENT

This work was supported by the Nuclear R&D program funded by the Ministry of Education, Science, and Technology (NO. 2010-0018524) and also by a grant from the Fundamental R&D Program for Technology of World Premier Materials funded by the Ministry of Knowledge Economy, Republic of Korea. This work was also supported by the National Research Foundation of Korea Grant funded by the Korean Government (MEST) (NRF-2009-C1AAA001-0093155).

REFERENCES

(1) Kang, K.; Meng, Y. S.; Breger, J.; Grey, C. P.; Ceder, G. *Science* **2006**, *311*, 977–980.
(2) Armand, M.; Tarascon, J. M. *Nature* **2008**, *451*, 652–657.
(3) Padhi, A.; Nanjundaswamy, K.; Goodenough, J. *J. Electrochem. Soc.* **1997**, *144*, 1188–1194.
(4) Li, G.; Azuma, H.; Tohda, M. *Electrochem. Solid-State Lett.* **2002**, *5*, A135–A137.
(5) Kim, J.; Seo, D. H.; Kim, S. W.; Park, Y. U.; Kang, K. *Chem. Commun.* **2010**, *46*, 1305–1307.
(6) Barker, J.; Saidi, M. Y.; Swoyer, J. US Patent PCT/US2010/0276632, 2007.
(7) Recham, N.; Chotard, J.; Dupont, L.; Delacourt, C.; Walker, W.; Armand, M.; Tarascon, J. *Nat. Mater.* **2009**, *9*, 68–74.
(8) Nyten, A.; Abouimrane, A.; Armand, M.; Gustafsson, T.; Thomas, J. O. *Electrochem. Commun.* **2005**, *7*, 156–160.
(9) Dominko, R.; Bele, M.; Gaberscek, M.; Meden, A.; Remskar, M.; Jamnik, J. *Electrochem. Commun.* **2006**, *8*, 217–222.
(10) Masquelier, C.; Padhi, A.; Nanjundaswamy, K.; Goodenough, J. *J. Solid State Chem.* **1998**, *135*, 228–234.
(11) Yin, S. C.; Grondey, H.; Strobel, P.; Anne, M.; Nazar, L. *J. Am. Chem. Soc.* **2003**, *125*, 10402–10411.
(12) Sauvage, F.; Quarez, E.; Tarascon, J. M.; Baudrin, E. *Solid State Sci.* **2006**, *8*, 1215–1221.
(13) Adam, L.; Guesdon, A.; Raveau, B. *J. Solid State Chem.* **2008**, *181*, 3110–3115.
(14) Nishimura, S.; Nakamura, M.; Natsui, R.; Yamada, A. *J. Am. Chem. Soc.* **2010**, *132*, 13596–13597.
(15) Zhou, H.; Upreti, S.; Chernova, N. A.; Hautier, G.; Ceder, G.; Whittingham, M. S. *Chem. Mater.* **2011**, *23*, 293–300.
(16) Gibot, P.; Casas-Cabanas, M.; Laffont, L.; Levasseur, S.; Carlach, P.; Hamelet, S.; Tarascon, J. M.; Masquelier, C. *Nat. Mater.* **2008**, *7*, 741–747.
(17) Park, Y. U.; Kim, J.; Gwon, H.; Seo, D. H.; Kim, S. W.; Kang, K. *Chem. Mater.* **2010**, *22*, 2573–2581.
(18) Nishimura, S.; Kobayashi, G.; Ohoyama, K.; Kanno, R.; Yashima, M.; Yamada, A. *Nat. Mater.* **2008**, *7*, 707–711.
(19) Masquelier, C.; Wurm, C.; Rodriguez-Carvajal, J.; Gaubicher, J.; Nazar, L. *Chem. Mater.* **2000**, *12*, 525–532.
(20) Wagemaker, M.; Ellis, B. L.; Lu tzenkirchen-Hecht, D.; Mulder, F. M.; Nazar, L. F. *Chem. Mater.* **2008**, *20*, 6313–6315.
(21) Wizansky, A. R.; Rauch, P. E.; DiSalvo, F. J. *J. Solid State. Chem.* **1989**, *81*, 203–207.
(22) Kim, S. W.; Kim, J.; Gwon, H.; Kang, K. *J. Electrochem. Soc.* **2009**, *156*, A635–A638.
(23) Roisnel, T.; Rodriquez-Carvajal, J. Transtec Publications; 1999: 2001; pp 118−123.
(24) Gwon, H.; Seo, D. H.; Kim, S. W.; Kim, J.; Kang, K. *Adv. Funct. Mater.* **2009**, *19*, 3285–3292.
(25) Kouass, S.; Guesmi, A.; Driss, A. *Acta Crystallogr.* **2010**, *C66*, i4–i6.
(26) Shannon, R.; Prewitt, C. T. *Acta Crystallogr., Sect. B: Struct. Sci.* **1969**, *25*, 925–946.
(27) Huang, Q.; Hwu, S. J. *Inorg. Chem.* **1998**, *37*, 5869–5874.
(28) Bih, H.; Saadoune, I.; Mansori, M. *J. Condens. Matter* **2006**, *7*, 74–77.
(29) Takahashi, M.; Tobishima, S.; Takei, K.; Sakurai, Y. *Solid State Ionics* **2002**, *148*, 283–289.
(30) Delacourt, C.; Poizot, P.; Tarascon, J. M.; Masquelier, C. *Nat. Mater.* **2005**, *4*, 254–260.
(31) Kobayashi, G.; Nishimura, S.; Park, M. S.; Kanno, R.; Yashima, M.; Ida, T.; Yamada, A. *Adv. Funct. Mater.* **2009**, *19*, 395–403.